IEEE Access
Multidisciplinary | Rapid Review | Open Access Journal

Received January 10, 2021, accepted January 25, 2021, date of publication February 5, 2021, date of current version February 17, 2021.

Digital Object Identifier 10.1109/ACCESS.2021.3057425

Research on a Novel Vascular Interventional Surgery Robot and Control Method Based on Precise Delivery

HONGBO WANG[1,2], (Member, IEEE), JINGYUAN CHANG[1,3], HAOYANG YU[3], HAIYANG LIU[3], CHAO HOU[2], AND HAIXIA LU[3]

[1]Parallel Robot and Mechatronic System Laboratory of Hebei Province, Yanshan University, Qinhuangdao 066004, China
[2]Academy for Engineering and Technology, Fudan University, Shanghai 200433, China
[3]Key Laboratory of Advanced Forging and Stamping Technology and Science, Ministry of Education, Yanshan University, Qinhuangdao 066004, China

Corresponding author: Chao Hou (27738821@qq.com)

This work was supported in part by the National Key Research and Development Program of China under Grant 2019YFB1311700, in part by the National Natural Science Foundation of China under Grant U1713219, and in part by the Shanghai Science and Technology Innovation Action Plan, China, under Grant 18441900700.

ABSTRACT In a vascular interventional surgery robot system, accurately pushing the guidewire into the patient-specific branch vessel is the core step of the entire operation, so it has become the focus of the master-slave co-control of the guidewire propulsion and manipulation mechanism. Some vascular interventional surgery robots have been used for delivery of the guidewire; however, problems such as the inability to reliably clamp the guidewire and the lack of accurate force feedback prevent doctors from using robots for accurate delivery. In addition, failure to disinfect surgical robots quickly and completely increases the risk of surgery. This article introduces a new type of master-slave vascular interventional robot with reliable clamping of the catheter/guidewire, accurate perception of the lead-in force of the guidewire for precise delivery and fast disinfection. In response to the problem of the nonlinear and uncertain disturbance of the catheter/guidewire resistance affecting the delivery mechanism, an adaptive sliding controller based on master-slave tracking is designed. Through experiments and analysis of the fuzzy sliding mode controller (FSMC) experimental platform, the results show that a vascular interventional robot control system with good tracking performance and strong robustness has been designed.

INDEX TERMS Adaptive sliding control, force feedback, precise delivery, quick disinfection, vascular interventional surgery robot.

I. INTRODUCTION

Vascular interventional surgery refers to a doctor's guided manipulation of catheters/guidewires in the blood vessels of the human body under a digital angiography machine for treatment of lesions, manipulation of embolisms of blood vessels, dissolution of blood clots, dilation of narrow blood vessels and other purposes. A vascular interventional surgery robot will ease patients' urgent needs for doctors, reduce the intensity of doctors' work, and improve the surgical efficiency and cure rates, which is currently a hot topic of domestic and foreign research and a very challenging subject in the field of robotics [1]. In a vascular interventional surgery robot system, according to a doctor's remote operation, insertion of a catheter/guidewire via a propulsion mechanism into a specific branch of a blood vessel is the key step throughout the operation and the main breakthrough in the research on vascular interventional surgery robots. Therefore, study of the guidewire propulsion mechanism and control system is one of the key scientific areas [2]–[7].

The research on guidewire propulsion mechanisms originated in the 1940s and 1950s, which can be divided into active wire propulsion mechanisms and passive wire propulsion mechanisms. For example, Sensei, a surgical robot from Hansen Medical in Canada, and Amigo, a surgical robot from Catheter Robotics in the United States, are both active types that enable insertion and extraction of active catheters/guidewires and bending of the head of the catheter.

The associate editor coordinating the review of this manuscript and approving it for publication was Luigi Biagiotti.

However, the passive wire guiding mechanism is widely adopted because of the easy-to-implement characteristics of the structure and control system [6]. The CorPath 200 wire propulsion system in Corindus, USA can feed balloons and stents along the guide to the position of vascular lesions and use the one-time-use shell to solve the partial disinfection problem. The wire propulsion mechanism developed by Professor Wang Shuguo of Harbin University of Technology, China, which adopts two motors to separately drive the catheter for axial feed and rotational motion, pushes the catheter by the friction drive of a roller [8]–[17]. Professor Wang Hongbo of Yanshan University developed a vascular interventional surgery robot catheter/guidewire propulsion mechanism and positioning robotic arm; this propulsion mechanism imitates the hand-propelled and rotation operations [1]–[3].

The control performance of surgical robots is directly related to the performance of the entire system or even determines the success or failure of surgery. SensAble of the United States has successfully developed a series of PHANTOM force feedback operating masters. The PHANTOM series main hands mainly include three types of products: the PHANTOM Desktop force feedback operating master, the PHANTOM Omni force feedback operating master and the PHANTOM Premium Force Feedback operating master, shown in Figs. 1-8. The PHANTOM Omni force feedback operating master and PHANTOM Desktop force feedback operating master both have 6 degrees of freedom and a 3D force feedback function.

The Premium series has three products: 1.0, 1.5, and 3.0. The Premium can feed back a wider range of forces and provide a larger workspace, and programming is easier and faster compared to the Desktop. The Phantom 1.5/6dof force feedback operation main hand can not only feedback the three-dimensional force but also reflect the three-dimensional torque, which better fits the actual conditions. Shanghai Jiaotong University in China has developed a 5 degrees of freedom force feedback master for celiac surgery. This master uses a motor for each degree of freedom to provide force feedback and can achieve the clamping operation of laparoscopic surgery by providing 1 clamping degree of freedom at the end. Harbin University of Technology has developed a force feedback master for master-to-slave operation, which adopts a string-based mixed structure and has 7 motional degrees of freedom, 3D force feedback functions, and a 100 mm × 100 mm × 100 mm working space. The ''Magic Hand'' robot master developed by Tianjin University is an improvement based on PHANTOM, has 7 degrees of freedom, and provides a feedback force of up to 12 N in 3 directions of movement via the installed motor. In addition, Southern Medical University, Fudan University Affiliated Hospital and other units have also started research work with PHANTOM as the robot master [17]–[20].

Based on the literature review and practical requirements, a new type of vascular interventional surgery robot master-slave design scheme is proposed in this article: It can reliably hold the catheter/guidewire, enable quick replacement of the catheter/guidewire, achieve rapid disinfection, and accurately detect the resistance of the catheter/guidewire during propulsion, which is amplified. The feedback, propulsion mechanism and rotational kinetic energy can be simultaneously decoupled from each other at the same time [1], [21]–[27]. The operating mechanism conforms to the doctor's operating habits and can provide effective feedback force information [13], [28]–[32]. Based on this scheme, a vascular interventional surgery robot is built, an adaptive sliding controller based on a PI sliding surface is designed, and experimental verification is carried out with a fuzzy sliding mode controller (FSMC) experimental platform.

II. MASTER-SLAVE SYSTEM ANALYSIS AND STRUCTURAL DESIGN

At present, the minimally invasive vascular interventional surgical robot is composed of three parts: (1) Medical imaging navigation system for visualization of the inside of the blood vessels. (2) Master-slave system to assist doctors in completing interventional surgery, which can perform catheter/guidewire delivery, withdrawal, rotation, etc. (3) Positioning system of the robotic arm for position adjustment of the slave hand delivery and reliable positioning of the end delivery device to meet the surgical needs. This article is based on an existing system; only the master-slave system is researched in this work.

The master-slave operating system mainly consists of the master-hand operating mechanism, the slave-hand propulsion mechanism and the control system. The doctor observes the patient's intravascular condition through medical imaging in an isolation chamber and controls the main master-hand operating mechanism to generate the operating signal [18]. The control system issues motion commands to the propulsion mechanism of the slave hand according to the operating signal to control the catheter/guidewire for delivery, and the detected catheter/guidewire resistance signal is simultaneously transmitted back to the master hand [19], [33], [34]. The master-hand end changes the excitation current of the magnetic powder clutch according to the signal and realizes force perception feedback, as shown in Fig. 1.

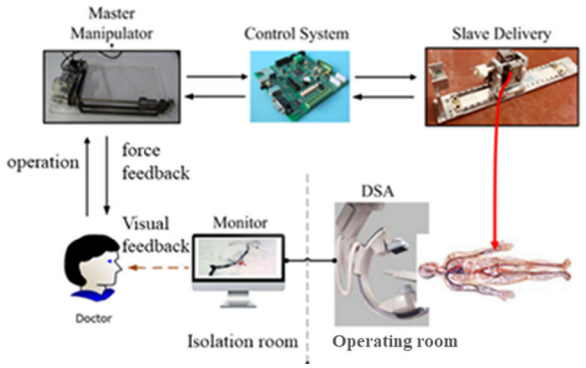

FIGURE 1. Master-slave system.

System Design Requirements:

(1) The slave-hand delivery mechanism must be able to accurately sense the contact force of the catheter/guidewire and the blood vessel wall. At the same time, the master-hand-end operating mechanism should be able to achieve resistance from the hand end in accordance with a certain proportion of the mapping ratio.
(2) The minimally invasive interventional robot system must have 2 degrees of freedom to decouple the delivery and rotation actions.
(3) The surface of the catheter and guidewire cannot be damaged.
(4) The slave-hand delivery structure should be easy to clean and the catheter/guidewire easy to replace [1], [4].

Design Parameters:

(1) The propulsion speed of the catheter/guidewire is better than 0 to100 mm/s, and the accuracy is less than 1 mm.
(2) The rotation speed of the catheter/guidewire is better than 0 to $40\pi\, rad/s$, and the accuracy is better than 3°.
(3) The maximum thrust is better than 5 N, and the rotational torque is at least $10mN \cdot m$.
(4) The volume is at most $50 \times 100 \times 90\, cm$, and the weight does not exceed 2 kg.

III. STRUCTURAL DESIGN AND SIMULATION ANALYSIS

A. PROPULSION MECHANISM OF THE SLAVE HAND

Consisting of a rack, a holder, and fixed and mobile fingers, the operating system of the slave-hand end is used to carry out axial advancement, withdrawal, and rotation of the catheter/guidewire [5], [33]. The propulsion mechanism of the slave hand is shown in Fig. 2.

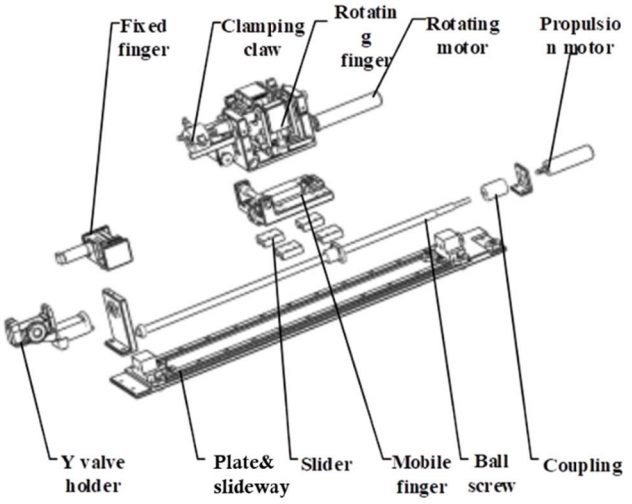

FIGURE 2. Propulsion mechanism of the slave hand.

The fixed frame is used to fix the Y valve. The fixed finger is used to guide and fix the catheter/guidewire when the mobile rack is withdrawn. As the core part of the structure, the moving rack is a composite structure, and the entire rack can be moved axially. The inner structure provides a rotation mechanism, which can achieve rotation of the catheter/guidewire [30]. The twisting mechanism is actuated by a belt with a special winding method, which can drive rotation of the catheter/guidewire through a tension wheel that causes the multiple drive-wheel clamping claws to rotate [14], [32]. This structure not only facilitates replacement of the catheter/guidewire and clamping claws but also avoids belt slip [2], [35], [36]. The rotation mechanism is shown in Fig. 3.

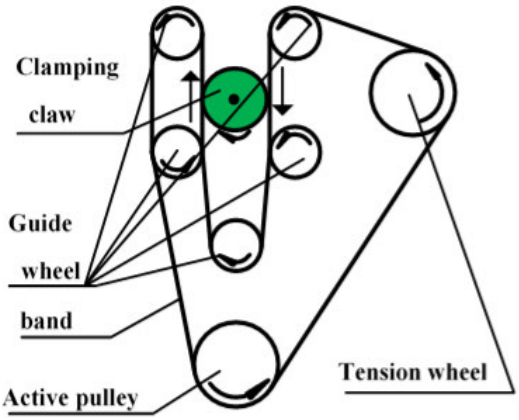

FIGURE 3. Belt winding principle.

The clamping claws use the movement of the guide sleeve to adjust the opening size for applying catheters/guidewires of different outer diameters, simultaneously changing the clamping force. The movement of the guide sleeve is achieved by a compression spring and tightening rope. In the natural state, the guide sleeve is pushed by the compression spring so that the clamping claws are tightened. In the working state, a motor (RE13-MR256CPT, Maxon, Switzerland)-driven tension rope precisely adjusts the guide sleeve position, making the clamping claw opening larger, to realize clamping or loosening of the catheter/guidewire with flexibility and reliability [3], [37]. The clamping claw structure is shown in Fig. 4. The clamping claw opening and closing principle is shown in Fig. 5.

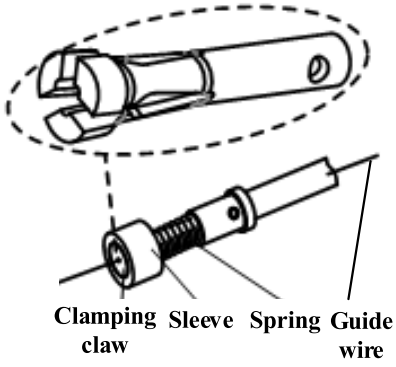

FIGURE 4. Clamping claw structure.

In addition to translation with the moving rack, this structure can also be deflected as a whole on the

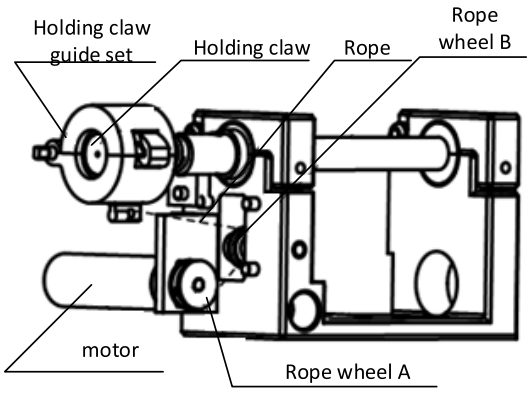

FIGURE 5. Clamping claw opening and closing principle.

mobile rack, forming a force amplification mechanism to amplify the resistance of the catheter/guidewire [15]. The tiny resistance is measured with a micro-pressure sensor (MDL: SBT674-2kg, Simbatouch, CN) below the rotation mechanism, which does not increase the complexity of the structure. The resistance detection mechanism is shown in Fig. 6.

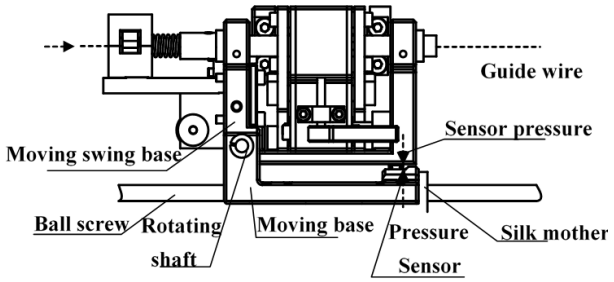

FIGURE 6. Resistance detection mechanism.

For easy cleaning of the clamping claws that directly contact catheters/guidewires, we design the clamping claw guide sleeve and upper swing base as a quick-to-dismantle structure, allowing the clamping claws to be quickly and easily installed and removed [15], [30]. The clamping claw removal structure is shown in Fig. 7.

B. MASTER-HAND OPERATING MECHANISM

Consisting of an operating sleeve, an operating shaft, a magnetic powder brake (CD-HSY-5, Lanling, CN), and so on, the master-hand-end mechanism is used to receive the operation commands of the doctor and feed the resistance of the catheter/guidewire back to the doctor [2], [33]. The master-hand-end operating mechanism is shown in Fig. 8.

The operating sleeve is the core component of the master-hand-end operating mechanism. The operating mechanism is exactly the same as the doctor's artificial way of advancing the catheter/guidewire. The operating sleeve moves to advance and withdraw the corresponding catheter/guidewire along the axial direction of the operating shaft. Six balls are placed between this sleeve and the operating axis to

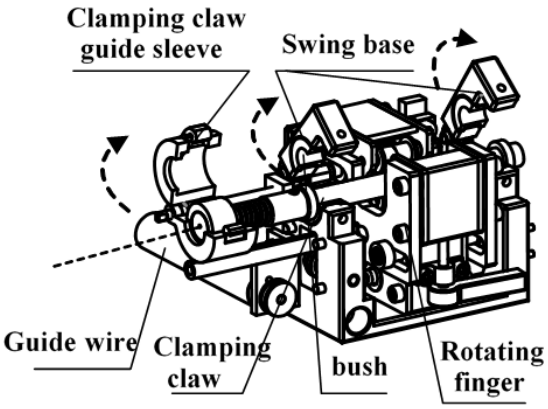

FIGURE 7. Clamping claw removal structure.

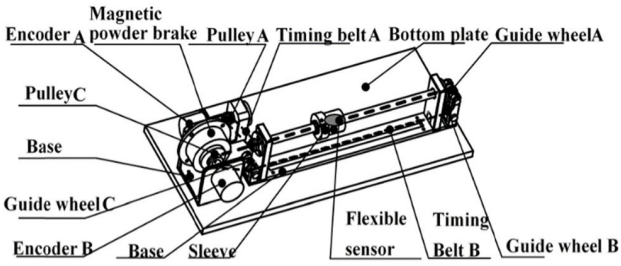

FIGURE 8. Master-hand-end operating mechanism.

reduce the friction between them. The resistance of the operating sleeve when it is moving is adjusted by the magnetic powder brake, which is the same resistance as for the catheter/guidewire. Its rotation with overall rotation of the operating axis corresponds to rotation operation of the catheter/guidewire. The flexible skin sensor on its surface is used to capture the doctor's clamping force to adjust the clamping force of the claws on the slave-hand-end propulsion system [30]. The operating sleeve axial advancement and force feedback structure are shown in Fig. 9.

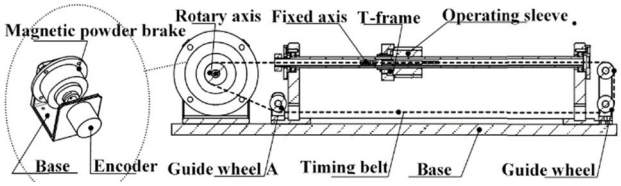

FIGURE 9. Operating sleeve axial advancement and force feedback structure.

C. SIMULATION ANALYSIS

The dynamic performance of the propulsion mechanism of the slave-hand end directly determines the accuracy and performance of the surgical robot. Motion simulation of the propulsion mechanism was carried out with the Adams soft-body simulation technology. Lightweight analysis of the mobile rack was performed using the ANSYS finite element

analysis, which reduces the mass of the moving rack while maintaining the strength [32], [36].

After converting the SolidWorks-built slave-hand-propelled mechanism model into Parasolid (*.x_t) format, we imported an Adams View module and customized the physical properties of the virtual prototype, including the material mechanics, mass and other physical parameters. At the same time, the constraint relationships of the propulsion structure were applied to add motion constraints. The model of the processed propulsion mechanism is shown in Fig. 10. In this article, most of the materials for the processed parts are made of hard aluminium, with an elastic modulus of $6.9 \times 10^{10} N/mm^2$; the specific physical parameters can be found in Table 1.

TABLE 1. Material performance parameters.

Material	Elastic modulus	Poisson's ratio	Density
Hard aluminum	$6.9x10^{10}$	0.33	$2.7x10^3$
Ball screw	$2.06x10^{11}$	0.29	$1.8x10^3$
Flexible coupling	$7.00x10^{10}$	0.33	$2.7x10^3$

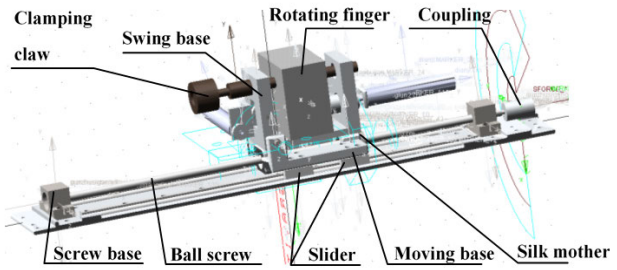

FIGURE 10. Propulsion mechanism model.

To simplify processing, most parts of the model are treated as ideal rigid bodies; that is, two points on a part cannot move relative to each other in simulation operations. The tangibly changing parts, such as the ball screw and elastic coupling, need to be treated as flexible bodies to meet the accuracy requirements.

According to the ball screw lead, the relationship between the displacement of the moving finger and the angular displacement of the ball screw in an ideal case can be calculated by the following formula:

$$\theta_m(t) = \frac{2\pi}{P_h} X(t);$$

where:

$\theta_m(t)$ – Angular displacement of the ball screw (rad);
P_h – Ball screw lead (mm);
$X(t)$ – Moving finger displacement (mm).

The relationship between the acceleration of the moving finger and the angular acceleration of the ball screw can be obtained by taking the derivative of the two sides of the above formula:

$$\ddot{\theta}_m(t) = \frac{2\pi}{P_h} \ddot{X}(t)$$

where:

$\ddot{\theta}_m(t)$ – Angular acceleration of the ball screw (rad/s^2);
P_h – Ball screw lead (mm);
$\ddot{X}(t)$ – Moving finger acceleration (mm/s^2).

Using a step function for the steering drive, the drive applies an angular speed at the input of the coupling. According to the mechanical parameters of the relevant material given in Table 1, the dynamic response curve of the moving finger is obtained. The moving finger displacement curve is shown in Fig. 11, and the acceleration curve is shown in Fig. 12.

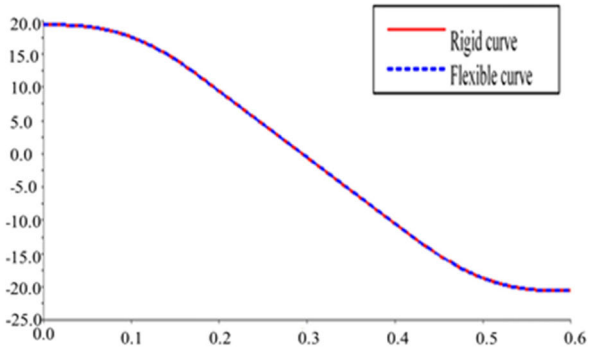

FIGURE 11. Moving finger displacement response curve.

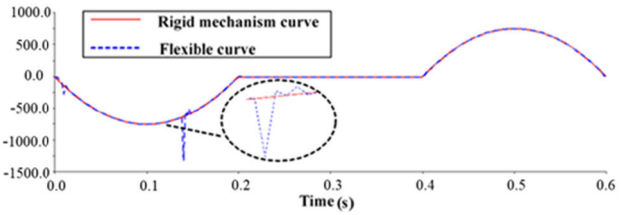

FIGURE 12. Moving finger acceleration response curve.

In comparison, the displacement response curves of the moving finger under the rigid and flexible body models almost coincide, which indicates that the ball screw and elastic coupling selected in this article can meet the stiffness requirements of the propulsion mechanism. The acceleration response curve in the rigid body model has significant local fluctuations, which may be a friction effect when the propulsion mechanism speeds up or slows down.

Leaving the other parameters unchanged while reducing the overall mass of the mobile rack by 10%, the acceleration response curve is shown in Fig. 13. A significant change occurs in the acceleration response curve of the propulsion mechanism by comparison. Thus, when we use the speed control mode, the mass has an impact on the acceleration

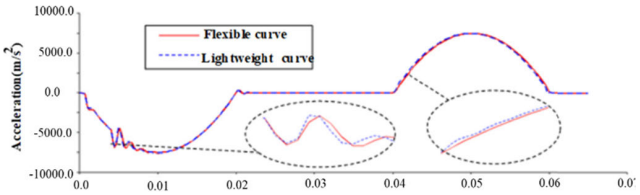

FIGURE 13. Lightweight mobile rack acceleration response.

response of the propulsion mechanism. Reducing the mass of the mobile rack improves the dynamic performance of the delivery mechanism.

To reduce the mass of the mobile rack, ANSYS/Workbench finite element topology optimization principles were used, and lightweight analysis was performed for the mobile rack moving base, moving swing base, rotating finger, fixed shaft and other components,. Under the premise of meeting the strength and stiffness requirements, the mass in the simulation calculation was reduced by a total of 0.117 kg, which is 15.32% of the mobile rack mass, as can be seen in Table 2.

TABLE 2. Lightweight mobile rack results.

Part	Moving base	Moving-finger-end support plate	Rotating finger support plate	Outside support plate
Original mass	0.12	0.162	0.024	0.034
Lightweight mass	0.08	0.107	0.012	0.024

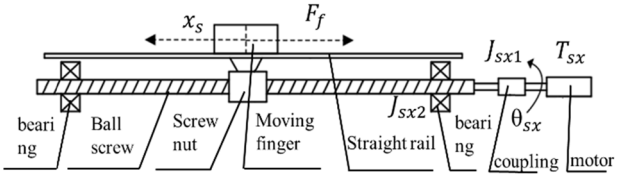

FIGURE 14. Axial motion dynamics model of the patient-end propulsion mechanism.

IV. CONTROLLER DESIGN

A. MOTION DYNAMICS MODELLING

The dynamic model of the axial motion of the patient-end propulsion mechanism is shown in Fig. 14.

Choosing a brushless servo motor as the propulsion mechanism to provide axial motion, the dynamic equation is

$$T_{sx} = J_s \frac{d^2\theta_{sx}}{dt^2} + B_s \frac{d\theta_{sx}}{dt} + T_{sx1} \tag{1}$$

The dynamic equation for the coupling is

$$T_{sx1} = J_{sx1} \frac{d^2\theta_{sx}}{dt^2} + T_{sx2} \tag{2}$$

The dynamic equation of the ball screw is

$$T_{sx2} = J_{sx2} \frac{d^2\theta_{sx}}{dt^2} + T_t \tag{3}$$

The relationship between the torque of the screw and thrust is

$$T_t = \frac{P}{2\pi \cdot \eta_1} F_t \tag{4}$$

The axial load of the screw is

$$F_t = m_t \frac{d^2 x_s}{dt^2} + F_f + F_e \tag{5}$$

The force relationship between the clamping claws and the guidewire is

$$F_f = \mu_\upsilon \cdot \frac{dx_s}{dt} + \mu_c \cdot m_t g \tag{6}$$

The relationship between the guidewire displacement and the corner of the screw is

$$x_s = \frac{p}{2\pi} \theta_{sx} \tag{7}$$

Combining (1)– (7), the relationship between the servo motor driving force moment and the guidewire displacement is

$$T_{sx} = \frac{2\pi}{p}\left[(J_s + J_{sx1} + J_{sx2}) + \frac{m_t}{\eta_1}\left(\frac{p}{2\pi}\right)^2\right]\frac{d^2 x_s}{dt^2} + \left(\mu_\upsilon \frac{p}{2\pi\,\eta_1} + B_s \frac{2\pi}{p}\right)\frac{dx_s}{dt} + \mu_c m_t g \frac{p}{2\pi \cdot \eta_1} \tag{8}$$

In formula (8), T_{sx} is torque of the servo motor, $N \cdot m$; p is the screw lead, mm; J_s is the motor rotational inertia, $kg \cdot m^2$; J_{sx1} is the coupling rotational inertia, $kg \cdot m^2$; J_{sx2} is the screw rotational inertia, $kg \cdot m^2$; m_t is the mass of the moving finger, kg; x_s is the axial propulsion displacement of the guidewire, mm; μ_υ is the viscous friction coefficient of the rails; μ_c is the Coulomb coefficient of friction for the rails; η is the positive efficiency of the screw; and B_s is the motor damping factor [38]. The dynamic model of the patient-end propulsion mechanism rotational motion is shown in Fig. 15.

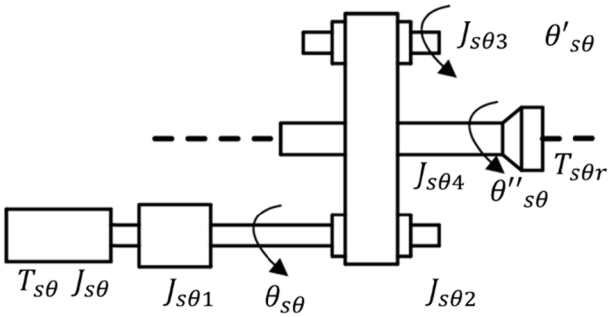

FIGURE 15. Dynamic model of the patient-end propulsion mechanism rotational motion.

The dynamic equation of the motor is

$$T_{s\theta} = J_s \frac{d^2\theta_{s\theta}}{dt^2} + B_s \frac{d\theta_{s\theta}}{dt} + T_{s\theta 1} \tag{9}$$

The dynamic equation for the coupling is

$$T_{s\theta 1} = J_{s\theta 1}\frac{d^2\theta_{s\theta}}{dt^2} + T_{s\theta 2} \tag{10}$$

The dynamic equation of the active wheel is

$$T_{s\theta 2} = J_{s\theta 2}\frac{d^2\theta_{s\theta}}{dt^2} + T_{s\theta 3} \tag{11}$$

The dynamic equation of the driven wheel is

$$T_{s\theta 3} = J_{s\theta 3}\frac{d^2\theta_{s\theta 1}}{dt^2} + T_{s\theta 4} \tag{12}$$

The dynamic equation for the clamping claws is

$$T_{s\theta 4} = J_{s\theta 4}\frac{d^2\theta_{s\theta 2}}{dt^2} + T_{s\theta r} \tag{13}$$

Combining (9) to (12), the relationship between the servo motor driving force moment and the doctor's action regarding the rotation of the guidewire is

$$T_{s\theta} = [(J_s + J_{s\theta 1} + J_{s\theta 2})\, i_{s\theta 1}\cdot i_{s\theta 2} + J_{s\theta 3} i_{s\theta 1} + J_{s\theta 4}\cdot i_{s\theta 1}\cdot i_{s\theta 2}] \times \frac{d^2\theta_{s\theta 2}}{dt^2} + B_s\cdot i_{s\theta 1}\cdot i_{s\theta 2} \tag{14}$$

In (14), J_s is the motor rotational inertia, $kg\cdot m^2$; $J_{s\theta 1}$ is the coupling rotational inertia, $kg\cdot m^2$; $J_{s\theta 2}$ is the active wheel rotational inertia, $kg\cdot m^2$; $J_{s\theta 3}$ is the driven wheel rotational inertia, $kg\cdot m^2$; $J_{s\theta 4}$ is the clamping claw rotational inertia, $kg\cdot m^2$; $i_{s\theta 1}$ is the transmission ratio of the active wheel and driven wheel; $\theta_{s\theta 1}$ is the active wheel rotation angle, rad; $\theta_{s\theta 2}$ is the driven wheel rotation angle, rad; and B_s is the motor damping factor.

B. ADAPTIVE SLIDING MODE CONTROLLER BASED ON A PI SLIDING SURFACE

When we established the axial motion dynamics of the patient-end propulsion mechanism in section A, we ignored the nonlinear disturbances. Because the wire itself is a flexible body with infinite degrees of freedom, in the process of delivering the guidewire to the target area, the positioning accuracy of the guidewire will be affected by a few uncertain factors such as the changes in the shape of the guidewire itself, friction between the guidewire and the walls of blood vessels and blood flow. Therefore, a new type of adaptive sliding mode controller based on a PI sliding surface is designed in this article [35], [36].

According to formula (8), we introduce interference items and represent the dynamic model of the axial motion of the propulsion mechanism as

$$T_{sx} = \frac{2\pi}{p}\left[(J_s + J_{sx1} + J_{sx2}) + \frac{m_t}{\eta_1}\left(\frac{p}{2\pi}\right)^2\right]\ddot{x} + \left(\mu_\upsilon\frac{p}{2\pi\cdot\eta_1} + B_s\frac{2\pi}{p}\right)\dot{x} + \mu_c m_t g\frac{p}{2\pi\cdot\eta_1} + \Delta \tag{15}$$

In formula (8),

$$\begin{bmatrix}\dot{x}_s(t)\\ \ddot{x}_s(t)\end{bmatrix} = \begin{bmatrix}0 & 1\\ 0 & -B_1/A_1\end{bmatrix}\begin{bmatrix}x_s(t)\\ \dot{x}_s(t)\end{bmatrix} + \begin{bmatrix}0\\ 1/A_1\end{bmatrix}T_{sx} - \begin{bmatrix}0\\ 1/A_1\end{bmatrix}(D_1 + \Delta) \tag{16}$$

$A_1 = (J_s + J_{sx1} + J_{sx2}) + \frac{m_t}{\eta_1}\left(\frac{p}{2\pi}\right)^2$; $B_1 = \mu_\upsilon\frac{p}{2\pi\cdot\eta_1} + B_s\frac{2\pi}{p}$; $D_1 = \mu_c m_t g\frac{p}{2\pi\cdot\eta_1}$; Δ is interference items.

The key step in the design of the sliding mode control is the design of the sliding surface $s(t)$. According to (16), the system is a second-order system. This article sets the controller based on the PI sliding surface. The tracking error of the PI sliding surface in space is defined as

$$s(t) = K_p e(t) + K_i\int e(\xi)d\xi \tag{17}$$

Combining (16) and (17),

$$s(t) = \begin{bmatrix}c & 1\end{bmatrix}\left(\begin{bmatrix}x_s\\ \dot{x}_s\end{bmatrix} - \begin{bmatrix}x_d\\ \dot{x}_d\end{bmatrix}\right) = (\dot{x}_s - \dot{x}_d) + c(x_s - x_d) \tag{18}$$

$$s'(t) = -\frac{B_1}{A_1}\dot{x}_s + c(\dot{x}_d - \dot{x}_s) - \ddot{x}_d + \frac{1}{A_1}T_{smc} - \frac{D_1 + \Delta}{A_1} \tag{19}$$

According to the index approach law, the sliding mode control rate is

$$U_{smc} = A_1 c(\dot{x}_d - \dot{x}_s) + A_1\ddot{x}_d + B_1\ddot{x}_s + D_1 + \Delta - k_1 s(t) - k_2 sign(s(t)) \tag{20}$$

In formula (20),

$$A_1 = (J_s + J_{sx1} + J_{sx2}) + \frac{m_t}{\eta_1}\left(\frac{p}{2\pi}\right)^2;$$

$$B_1 = \mu_\upsilon\frac{p}{2\pi\cdot\eta_1} + B_s\frac{2\pi}{p};\quad k_1 > 0;\ k_2 > 0.$$

To verify the stability of the system, according to the Lyapunov theorem,

$$\dot{V}_t = \sigma(t)\left(-\frac{k_1}{A_1}s(t) + \frac{k_2}{A_1}sign(s(t)) - \frac{1}{A_1}\dot{\Delta}\right) \le 0 \tag{21}$$

According to formula (21), the control rate we designed can make the system error tend to stability for a limited time.

As for the uncertainty of the external disturbance, we estimate the adaptive parameter k_2.

$$k_2(t) = \begin{cases}\mu/s(t)/ & /s(t)/ > \varepsilon\\ 0 & /s(t)/ < \varepsilon\end{cases} \tag{22}$$

For the linear and nonlinear parts of the patient-end propulsion mechanism dynamics, the control rate is divided into equivalent control and robust control:

$$U_{ASMC} = U_{eq} + U_r \tag{23}$$

The equivalent control volume U_{eq} is as follows:

$$U_{eq} = \left[(J_s + J_{sx1} + J_{sx2}) + \frac{m_t}{\eta_1}\left(\frac{p}{2\pi}\right)^2\right]s^2 + \left[\mu_\upsilon\frac{p}{2\pi\cdot\eta_1} - ((J_s + J_{sx1} + J_{sx2}) + \frac{m_t}{\eta_1}\left(\frac{p}{2\pi}\right)^2\cdot c - k_1)\right]s + k_1 s + k_{1c} \tag{24}$$

The robust control amount U_r is as follows:

$$U_r = (K_P + K_i)sign(s) \tag{25}$$

The axial motion dynamics equation for the patient-end propulsion mechanism is

$$x_s = \frac{1}{A_1 s^2 + B_1 s}(T_{sx} - D_1 - \Delta) \tag{26}$$

In formula (26):

$A_1 = (J_s + J_{sx1} + J_{sx2}) + \frac{m_t}{\eta_1}\left(\frac{p}{2\pi}\right)^2; B_1 = \mu_\upsilon \frac{p}{2\pi \cdot \eta_1} + B_s \frac{2\pi}{p}; D_1 = \mu_c m_t g \frac{p}{2\pi \cdot \eta_1}$.

With the introduction of the adaptive sliding controller, the principle of propulsion position control of the microinvasive vascular interventional robot guidewire is shown in Fig. 16.

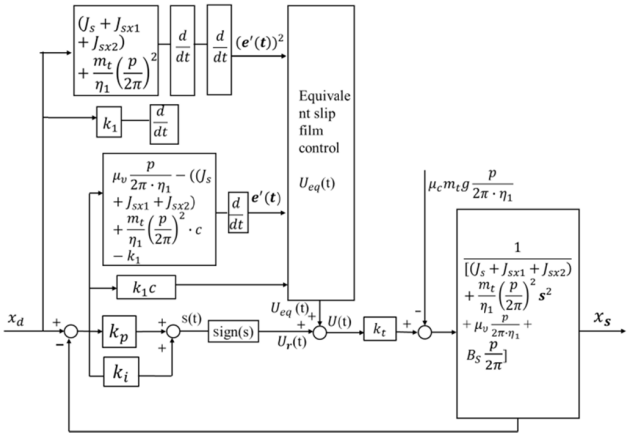

FIGURE 16. Wire adaptive sliding position control scheme.

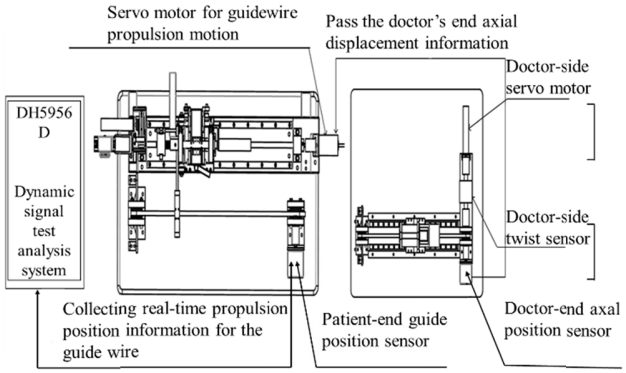

FIGURE 17. Working principle of the test bench.

V. EXPERIMENTAL RESEARCH

A. FSMC GUIDEWIRE POSITION CONTROL PERFORMANCE EXPERIMENT

The working principle of the test bench for the control algorithm that we used in this article is shown in Fig. 17. The doctor-end operating mechanism gives the patient preset input signal and uses the dynamic signal collector to collect the guidewire propulsion position information of the patient-end propulsion mechanism [35]. A photo of the test bench is shown in Fig. 18. Table 3 indicates the relevant technical parameters of the test bench designed in this article.

A sine signal is the classic signal for master-slave system performance testing. The quality of the sine response can determine the performance of the guidewire propulsion position control system. Under different sine responses, different manifestations of the wire position control system are added to the test scheme, and research was performed after designing the test schemes shown in Table 4 [37], [39].

In the FSMC guidewire position control performance test, the effectiveness of the control algorithm designed in this article was verified by contrasting the wire position accuracies when using proportional-integral-derivative (PID) control or adaptive fuzzy sliding control. Because of the limit of the overall size of the delivery mechanism structure, the effect of the designed control algorithm on the control accuracy of the guidewire propulsion position was not verified by directly observing the sine response signals. Thus, the error curve of the input position and output position is given to observe the control effect of the control algorithm [40]–[42].

TABLE 3. Indicator parameters of the FSMC performance test platform.

Name	Parameters and descriptions
Servo motors of the guidewire propulsion	Rated voltage: 12 V, rated speed: 10200 rpm, rated torque: 2.45 mNm, rated current: 0.331 A, slowdown ratio: 29:1
Doctor-end servo motor	Rated voltage: 12 V, rated speed: 10200 rpm, rated torque: 2.45 mNm, rated current: 0.331 A, slowdown ratio: 279:1
Doctor-end torque servo	Range: 5 $N \cdot m$, output sensitivity: 1.0 mV/V, linearity: $\pm 0.3\% F.S.$, excitation voltage: $24VDC$, output: $0 \pm 5\ V$, operating temperature range: $-30\,℃$ to $+70\,℃$
Doctor-end axial position sensor	Supply voltage: $DC\ 5 \pm 0.5\ V$, operating temperature: -20 to $80℃$, linearity: $0.03\% F.S.$, measurement accuracy: 8 bits/turn, measurement range: 1-65536 turns.
Patient-end guidewire position sensor	Supply voltage: $DC\ 5 \pm 0.5\ V$, operating temperature: -20 to $80℃$, linearity: $0.03\% F.S.$, measurement accuracy: 8 bits/turn, measurement range: 1-65536 turns.

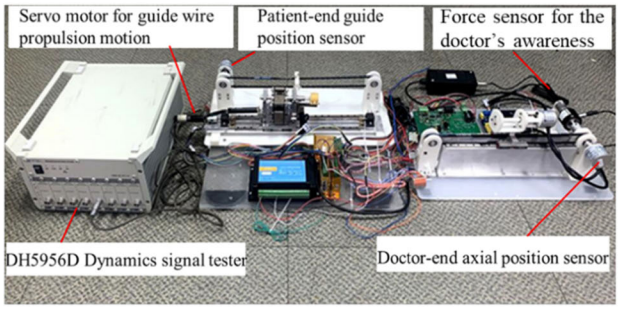

FIGURE 18. Working platform.

TABLE 4. Wire adaptive fuzzy sliding mode position control design scheme.

The signal entered				
Sine response	amplitude	45 (7.85 *mm*)	frequency	0.05 Hz
	frequency	0.05 Hz	amplitude	22.5 (3.93 *mm*)
		0.04 Hz		33.75 (5.89 *mm*)
		0.03 Hz		45 (7.85 *mm*)

The sine input signals used for the experimental test of the vascular intervention robot system are shown in Table 5. The sine signal magnitudes were 7.85 *mm* and 3.49 *mm* for frequencies of 0.05 *Hz*, 0.04 *Hz*, 0.03 *Hz*, and for the frequency of 0.05 *Hz*, the magnitudes were 3.49 *mm*, 5.89 *mm*, and 7.85 *mm*. The experimental accuracy curves of the corresponding wire position control are shown in Figs. 19-23.

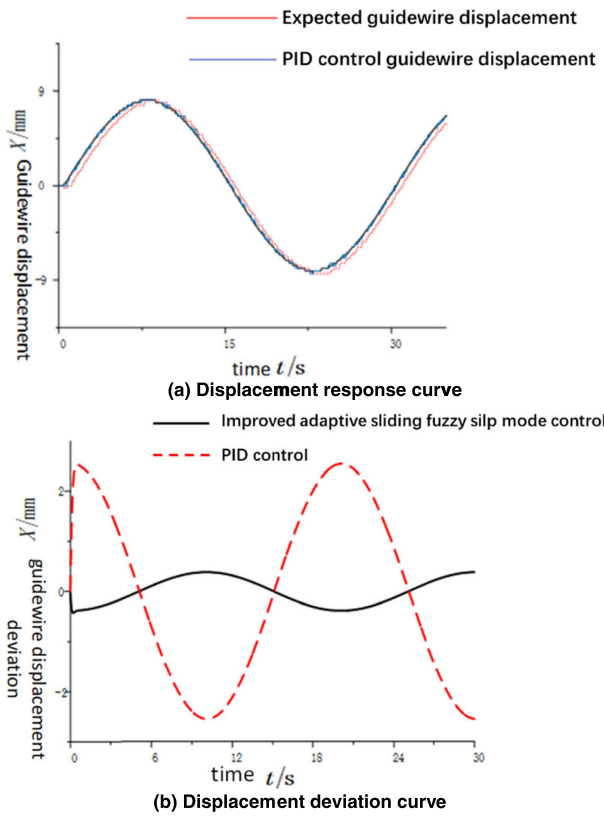

FIGURE 19. Amplitude: 7.85 mm, frequency: 0.03 Hz.

From Figs. 19-23, the axial propulsion position deviations under the sine input signals of the wire position control schemes are shown in Table 5, where the wire axial position deviation elimination rate = (1 − corresponding error of the FSMC controller)/ corresponding error of the PID controller × 100%, the maximum deviation = (input signal − output signal) $_{\text{Absolute}}$, and the average deviation = ((input signal) $_{\text{absolute}}$ − (output signal) $_{\text{absolute}}$)$_{\text{Average}}$.

TABLE 5. Indicator parameters of the FSMC performance testing experiment platform.

Input signal		Average location deviation of PID controller/mm	Average position deviation of FSMC/mm	Average position deviation elimination rate/%	Maximum PID position deviation/mm	Maximum position deviation of FSMC/mm	Maximum position deviation elimination rate/%	Variance of PID position deviation	Variance of FSMC position deviation
π/4 (7.85 mm)	0.05 Hz	0.60006	0.26051	55.12	0.60091	0.34229	50.03	0.53227	0.50311
	0.04 Hz	0.40113	0.06745	80.34	0.59336	0.16631	42.00	0.56555	0.48166
	0.03 Hz	0.50884	0.42213	77.65	0.89220	0.49331	41.01	0.57113	0.48882
0.05 Hz	π/8 (3.93 mm)	0.40337	0.07001	74.01	0.73229	0.34665	49.67	0.56033	0.43100
	π/6 (5.89 mm)	0.41422	0.06625	76.01	0.89001	0.38776	49.26	0.55053	0.45022
	π/4 (7.85 mm)	0.60006	0.21131	55.12	0.60091	0.33166	50.03	0.56167	0.56122

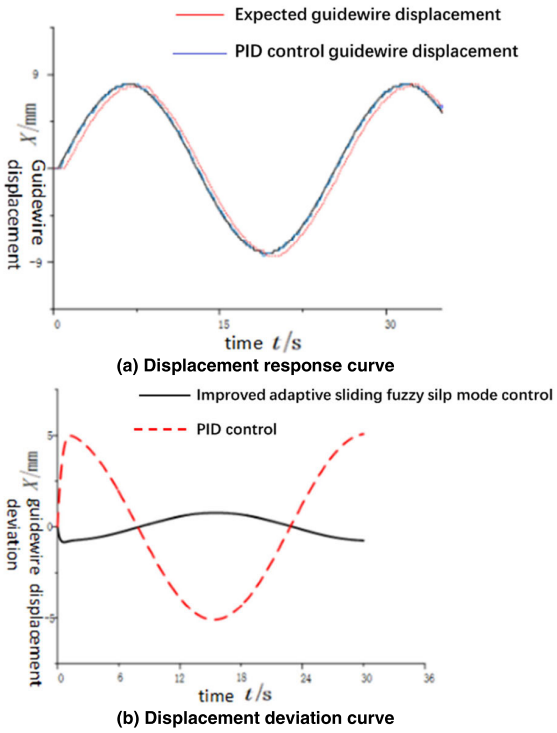

FIGURE 20. Amplitude 7.85 mm, frequency 0.04 Hz.

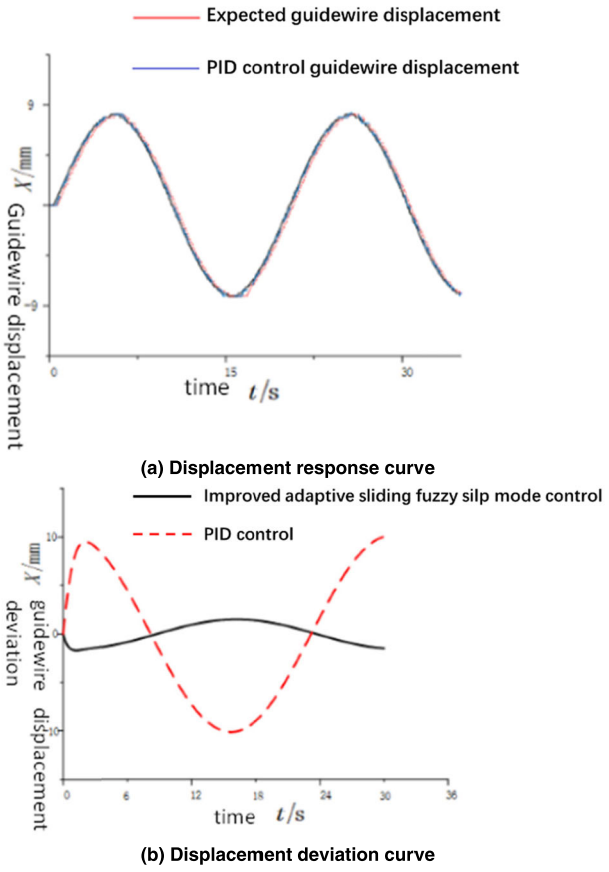

FIGURE 21. Amplitude 7.85 mm, frequency 0.05 Hz.

According to Figs. 19-23 and Table 3, compared with the proposed control strategy for master-slave position tracking

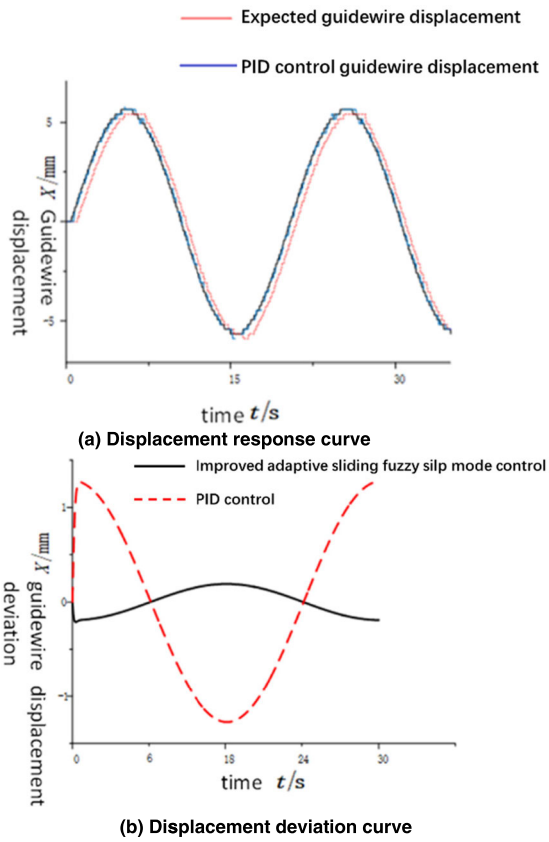

FIGURE 22. Amplitude 5.89 mm, frequency 0.05 Hz.

of the guidewire, the control performance of the guidewire delivery position using only the existing PID controller is relatively poor. The system's guidewire master-slave positioning deviation fluctuates between 0.4 mm and 0.65 mm. When the sinusoidal response amplitude and frequency are large, the guidewire position control system using only the PID controller cannot meet the demand for high-precision position control of the guidewire in vascular interventional surgery. With the introduction of the FSMC controller, the position control performance of the guidewire can be greatly improved; the positioning deviation fluctuates between 0.07 mm and 0.3 mm, and the error elimination rate of the system relative to the PID controller fluctuates between 80% and 50%. In addition, after the introduction of the FSMC controller, the variance in the position deviation is smaller than that with the PID controller, the data fluctuation is small, and the control accuracy of the system is improved.

B. FORCE FEEDBACK PERFORMANCE EXPERIMENT

To verify the force feedback performance of the designed vascular interventional surgery robot, a time-varying force experiment was carried out. The force feedback experimental device is shown in Figs. 24 and 25: The vascular interventional surgery robot was placed horizontally with respect to the hand, and the guidewire (ATW-595-ME014, Cordis Corporation, USA) was passed through the clamping claw and extended forward to the front end of the Y valve holder.

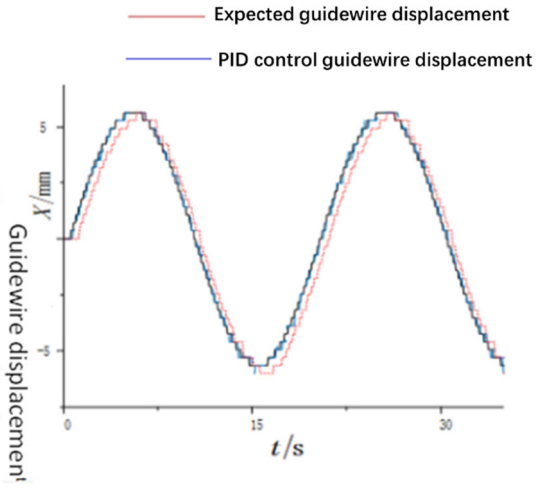

(a) Displacement response curve

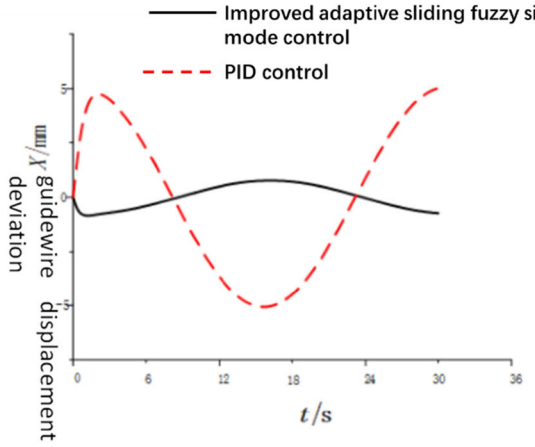

(b) Displacement deviation curve

FIGURE 23. Amplitude 3.93 mm, frequency 0.05 Hz.

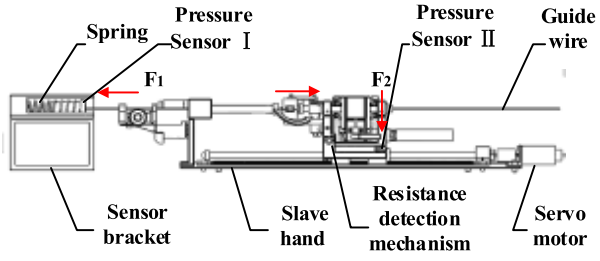

FIGURE 24. Force feedback experimental principle.

A sensor holder was placed in front of the Y valve holder. Pressure sensor I (MDL: SBT674-2kg, Simbatouch, CN) was connected to the sensor holder by a spring, and the axis of the sensor was kept on the same straight line as the guidewire. The servo motor drove forward movement, which then drove the guidewire to push pressure sensor I forward, and pressure sensor I recorded the change in the force at the tip of the guidewire. At the same time, the tip force of the guidewire was transmitted to pressure sensor II (MDL: SBT674-2kg, Simbatouch, CN) through the resistance detection mechanism of the surgical robot, and pressure sensor II recorded the measured force signal simultaneously.

By comparing force F1 of the guidewire tip with force F2 measured by the resistance detection mechanism and analysing the relationship between the two, we can evaluate the force feedback performance. The experimental results are shown in Fig. 26.

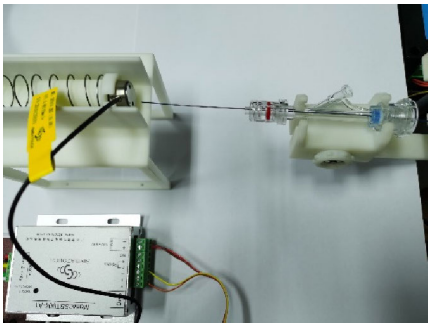

FIGURE 25. Force feedback experimental device.

Under the action of a time-varying force, the resistance detection mechanism can more accurately detect the tip force of the guidewire and reflect its changing trend. When the tip of the guidewire stably touches the object, the resistance detection mechanism can amplify this force, with a magnification factor of $K_1 = F_2/F_1$. The factor is between 1.86 and 1.92, which is in line with the expected target.

To verify the stability of the master-slave interaction when the above force feedback exists, while performing the above experiments, the force established by the master hand was recorded, that is, force signal F3 generated by the magnetic powder clutch at the master hand was collected. By comparing the changes of the master-end force signal F3 and the slave-end force signal F2, the stability of the master-slave system can be evaluated, as shown in Fig. 27.

The analysis shows that when force feedback exists, the slave-hand-end resistance detection mechanism can stably detect the tip force of the guidewire; at the same time, the amplified feedback force is processed by the control system and transmitted to the magnetic powder clutch at the master hand, establishing a stable force, which can effectively assist the doctor in the operation. Although a certain time lag exists between the master end and slave end, it is controlled within an acceptable range. Therefore, we suppose that when force feedback exists, the interaction between the master end and slave end is relatively stable.

C. PRECISE GUIDEWIRE DELIVERY EXPERIMENT

To verify whether the designed vascular interventional surgery robot can effectively assist the doctor in an operation, an experiment was conducted to test whether the guidewire can be accurately delivered to the target location. Ten testers were randomly selected to operate the vascular interventional surgery robot to deliver the guidewire (ATW-595-ME014, Cordis Corporation, USA) from the starting position of the human heart model to the target position, as shown in Fig. 28.

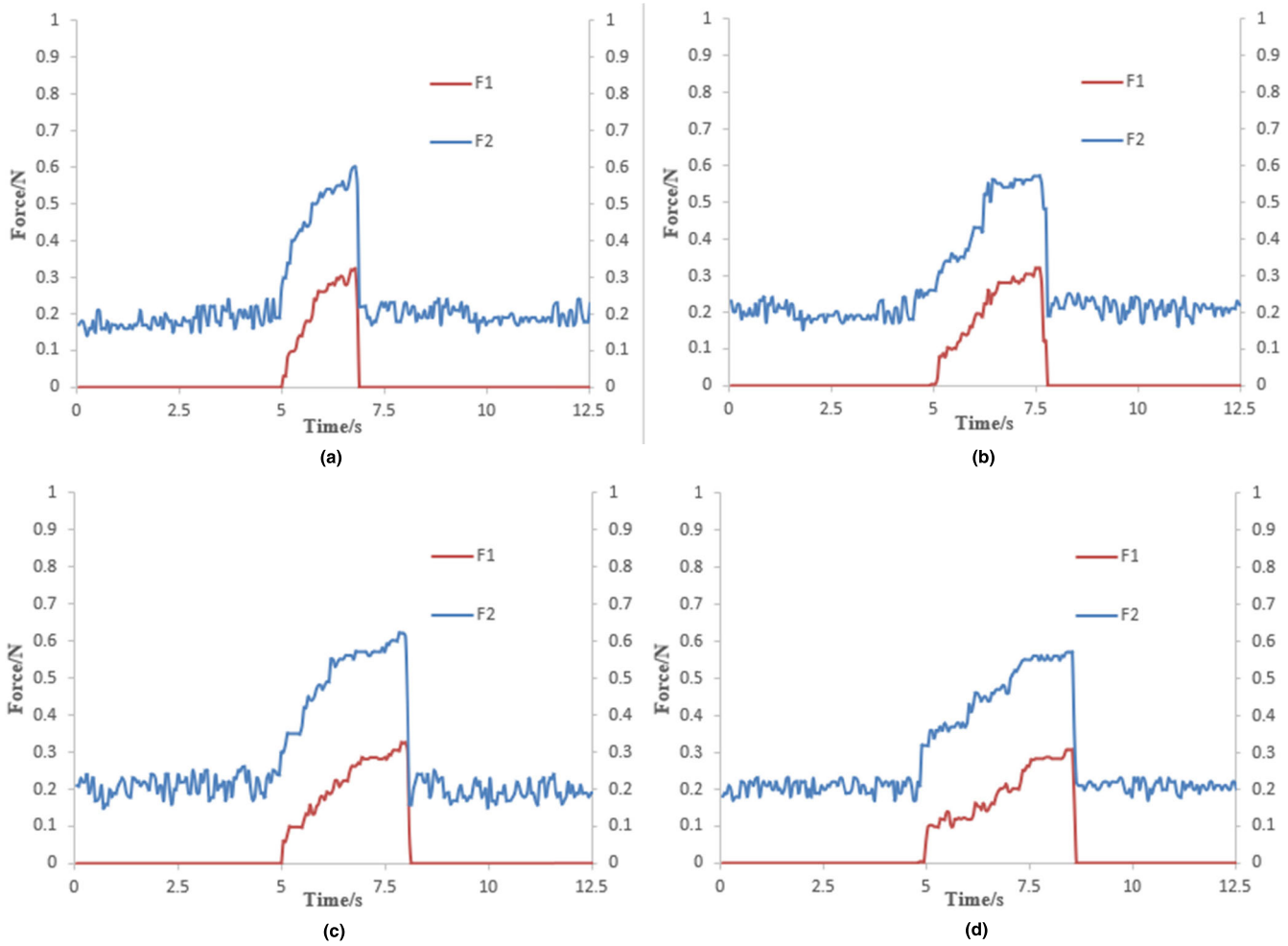

FIGURE 26. Force feedback experimental data.

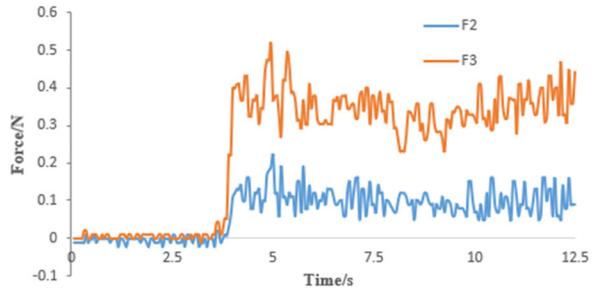

FIGURE 27. Master-slave force signal.

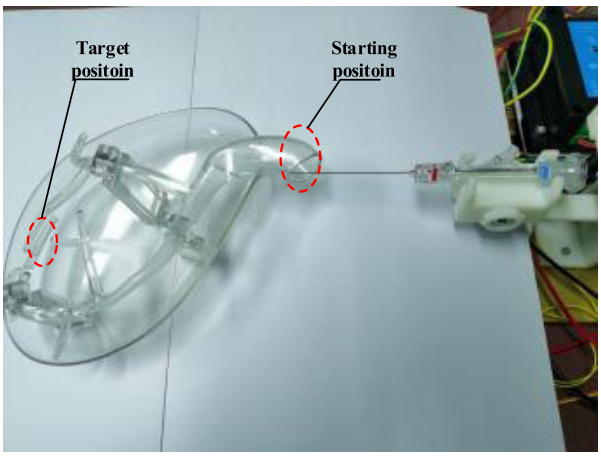

FIGURE 28. Precise guidewire delivery experimental device.

In this experiment, each tester operated the device 10 times and recorded the position of the guidewire and the maximum tip force of the guidewire. For each measurement, the distance from the starting position to the target position of the heart model was 250 mm. The actual delivery distance of the guidewire can be obtained by the encoder (RS485-RTU, Realwetech, CN) in the robot. The position of the guidewire can be obtained by comparing the two. The tip force of the guidewire can be measured by the resistance detection mechanism. The experimental results are shown in Fig. 29 and Table 6.

Fig. 29 shows that the maximum position error of the 10 testers in the guidewire delivery experiment did not exceed

TABLE 6. Maximum force of the guidewire tip.

	1	2	3	4	5	6	7	8	9	10
Maximum force	0.40	0.16	0.48	0.25	0.13	0.40	0.36	0.24	0.29	0.16

FIGURE 29. Guidewire position error.

2 mm, only one had a minimum position error of more than 0.5 mm, and the rest were less than 0.5 mm. The average position error did not exceed 1.5 mm. The average position error of 6 testers is approximately 1 mm. Table 6 shows that in the process of delivering the guidewire, the maximum force of the guidewire tip touching the blood vessel wall was usually not more than 0.4 N, and only one person had a maximum force of 0.48 N.

Considering that none of the 10 testers are professionally trained interventional doctors and that the material used for the key components of the vascular interventional surgery robot prototype was resin (WeNext8000&7500, WeNext Technology, CN), whereas in actual surgery, professional doctors will use high hardness materials such as aluminium alloy, we suppose that the designed vascular interventional surgery robot can assist doctors in accurately delivering the guidewire and that under the protection of the robot force feedback mechanism, it can prevent the tip of the guidewire from piercing the blood vessel wall.

VI. CONCLUSION

Vascular disease mortality is the leading cause of death in humans and is increasing year by year. Interventional surgery can cause serious harm to the patient, so introducing robotic technology to assist doctors to complete minimally invasive vascular interventional surgery has become an urgent need in the global medical device market. This article focuses on the core problems of lack of accurate delivery, force feedback and quick disinfection; low propulsion position accuracy; and low anti-jamming capability, which are common in the existing vascular interventional surgery robots. The main research results of this article are summarized below:

(1) According to the existing problems of surgical robots, combined with the specific requirements of the surgical procedures, a new vascular interventional surgery robot system with precision delivery of the catheter/guidewire has been designed, which has one-time-use, grip-adjustable clamping claws; can solve the problems of disinfection, slip, injury to the guidewire and so on; and can provide accurate force feedback, including for the main-hand operating mechanism and the slave-hand propulsion mechanism.

(2) The influence of the mass and stiffness on the dynamic characteristics of the propulsion mechanism was studied, and the mass was found to be the key factor that affects the dynamic characteristics of the propulsion mechanism. On this basis, lightweight analysis of key parts of the mobile rack was carried out by the finite element method, and the mass of the mobile rack was reduced by 15.32%, which improved the dynamic characteristics of the propulsion mechanism. Then, finite element analysis of clamping claws of different shapes and different opening angles was carried out, and an optimal optimization scheme was selected.

(3) In view of the nonlinear and uncertain disturbance of the catheter/guidewire resistance, which affects the delivery mechanism, an adaptive sliding controller based on master-slave position tracking with strong robustness has been designed. By comparing the traditional PID control with the adaptive sliding mode control designed in this article, the adaptive sliding mode control algorithm is found to reduce the influence of uncertainty on the stability of the system, reduce the control deviation, and improve the response speed, robustness and accuracy of the control system.

(4) According to the force feedback mechanism of surgical robots, a series of experiments were carried out. Through the analysis of experimental data, the force feedback performance and the stability of the master-slave interaction when force feedback exists were verified. We conducted experiments on the human heart model based on the robot. The results show that the designed vascular interventional surgery robot can effectively assist the doctor in accurately delivering the guidewire, and under the protection of the robot force feedback mechanism, it can prevent the tip of the guidewire from piercing the blood vessel wall.

REFERENCES

[1] H. B. Wang, "Minimally invasive vascular intervention alsterilised robot catheter and lead silk spin propulsion mechanism," China Patent 109 821 137 A, May 31, 2019.
[2] H. B. Wang, "A minimally invasive vascular intervention alsterilised robot catheter and wire propulsion mechanism," China Patent 109 821 138 A, May 31, 2019.
[3] H. Wang, "Minimally invasive vascular intervention surgery robot catheter/wire rotating mechanism and propulsion device," China Patent 108 704 214 A, Oct. 26, 2018.

[4] S. P. Han, L. Wang, and L. X. Ren, "Vascular intervention surgery robot guide wire/catheter control device," China Patent 108 514 448 B, Feb. 7, 2020.
[5] Y. Li, M. Fang, Z. Xi, J. Tu, and Y. Cheng, "An interventional vascular microsurgery robot," China Patent 110 664 489 A, Jan. 10, 2020.
[6] L. Li, T. H. Wang, and Y. Z. Tian, "A minimally invasive vascular interventional surgical robot-assisted wire inlet device," China Patent 110 464 967 A, Nov. 11, 2019.
[7] L. Yang, "A vascular intervention robot," China Patent 107 049 500 B, Oct. 29, 2019.
[8] X. Xie, "A vascular interventional surgical robot," China Patent 110 327 116 A, Oct. 15, 2019.
[9] L. Li, T. Wang, and Y. Tian, "Robotic wire feeding device for minimally invasive vascular interventional surgery, has guide wire axial movement component and guide wire circumferential movement component that are fixedly installed on bottom support component," China Patent 110 464 967 A, Nov. 19, 2019.
[10] T. Huang, "Interventional surgery robot reciprocating movement device, has clamping component for driving transverse reciprocating movement of first drive component, where clamping component drives reciprocating movement of second drive component," China Patent 110 236 680 A, Sep. 17, 2019.
[11] M. Deng, "Robot system for vascular interventional surgery, has base that is provided with auxiliary bracket whose upper is provided with guide sleeve, and duct that is sequentially passed through tube perforation and guide sleeve," China Patent 110 101 454 A, Aug. 9, 2019.
[12] G. Wang, L. Wang, Y. Zhang, W. Yan, F. Ou, and S. Han, "Design and analysis of vascular interventional surgical robot based on bionic fingers," *Mach. Tool Hydraul.*, vol. 47, no. 9, pp. 81–84, May 2019.
[13] X. Duan, Y. Chen, and H. Yu, "Design of the control system and home point positioning device for minimally invasive vascular interventional surgery robot," *Robot*, vol. 34, no. 2, pp. 129–136, Mar. 2012, doi: 10.3724/sp.j.1218.2012.00129.
[14] Z. Chen, M. Shen, and Q. S. Lu, "Advances in the study of robot-assisted vascular interventional therapy," *J. Interventional Radiol.*, vol. 27, no. 1, pp. 1–4, Jan. 2018, doi: 10.3969/j.issn.1008-794X.2018.01.001.
[15] D. Liu and Z. Q. Ni, "Surgical evaluation of vascular intervention robot system," *J. Tissue Eng. Reconstructive Surg.*, vol. 10, no. 1, pp. 19–21, Feb. 2014.
[16] X. M. Zhao, J. K. You, H. Liu, and H. Y. Li, "Minimally invasive vascular intervention surgery catheter-assisted robot self-straightening fuzzy PID control," *Chin. J. Biomed. Eng.*, vol. 33, no. 1, pp. 123–127, Feb. 2014.
[17] C. Y. Wang, "Overview of the development of medical surgical robots," *Tool Technol.*, vol. 50, no. 7, pp. 3–12, Jun. 2016.
[18] S. X. Guo, "Analysis of the current situation of intervention techniques in the robot-assisted vascular cavity," *Life Sci. Instrum.*, vol. 11, no. 5, pp. 3–12, 2013.
[19] Z. Q. Feng, "The master-slave interaction control method and realization of minimally invasive vascular intervention al-robot," *J. Automat.*, vol. 42, no. 5, pp. 696–705, Apr. 2016.
[20] Q. S. Lu, "Discussion on interventional surgical robot stoics in vascular cavity," *Chin. J. Vascular Surg.*, vol. 10, no. 4, pp. 237–239, Dec. 2018.
[21] H. Chen, L. Liu, and T. Cao, "Study on interventional robot kinematics and trajectory planning," *Elect. Mech. Eng.*, vol. 31, no. 6, pp. 679–683, Jun. 2014.
[22] F. Jiang, C. Y. Huang, Y. J. Wang, and Y. D. Hu, "Study on the effect of vascular structure on the outflow field of vascular robot," *Sci. Technol. Eng.*, vol. 14, no. 2, pp. 8–13, Jan. 2014.
[23] C. Ji, "A review of cardiovascular minimally invasive interventional catheter control techniques," *Robot. Appl.*, no. 6, pp. 25–33, Nov. 2011.
[24] W. Y. Xu, "Report on clinical application of vascular intervention robot," *Chin. J. Vascular Surg.*, vol. 6, no. 1, pp. 16–18, Mar. 2014.
[25] B. Jia, Z. Tian, W. Lu, and D. Liu, "Experimental study of remotely operated vascular intervention robot," *Chin. J. Minimally Invasive Neurosurg.*, vol. 17, no. 5, pp. 221–224, May 2012.
[26] R. Beyar, L. Gruberg, D. Deleanu, A. Roguin, Y. Almagor, S. Cohen, G. Kumar, and T. Wenderow, "Remote-control percutaneous coronary interventions," *J. Amer. College Cardiol.*, vol. 47, no. 2, pp. 296–300, Jan. 2006, doi: 10.1016/j.jacc.2005.09.024.
[27] C. Riga, C. Bicknell, N. Cheshire, and M. Hamady, "Initial clinical application of a robotically steerable catheter system in endovascular aneurysm repair," *J. Endovascular Therapy*, vol. 16, no. 2, pp. 149–153, Apr. 2009, doi: 10.1583/08-2651.1.
[28] J. Guo, "A novel robotic catheter system with force and visual feedback for vascular interventional surgery," *Int. J. Mechatron. Autom.*, vol. 2, no. 1, pp. 15–24, May 2012, doi: 10.1504/ijma.2012.046583.
[29] Y. Wang, S. Guo, N. Xiao, Y. Li, and Y. Jiang, "Surgeons' operation skill-based control strategy and preliminary evaluation for a vascular interventional surgical robot," *J. Med. Biol. Eng.*, vol. 39, no. 5, pp. 653–664, Oct. 2019, doi: 10.1007/s40846-018-0453-3.
[30] X. Bao, S. Guo, L. Shi, and N. Xiao, "Design and evaluation of sensorized robot for minimally vascular interventional surgery," *Microsyst. Technol.*, vol. 25, no. 7, pp. 2759–2766, Jan. 2019, doi: 10.1007/s00542-019-04297-3.
[31] Z. Q. Feng, "Design and control of minimally invasive vascular interventional surgical robot system," in *Proc. China Automat. Soc. Control Theory Prof. Committee, China Soc. Syst. Eng.*, 2013, pp. 1074–1079.
[32] H. Wang, X. Wang, B. Guan, J. Chang, H. Yu, and H. Tian, "Design of a positioning manipulator for minimally invasive vascular interventional surgery robot system," in *Proc. IEEE Int. Conf. Mechatronics Autom. (ICMA)*, Changchun, China, Aug. 2018, pp. 308–312.
[33] H. Liu, H. Wang, X. Yang, Z. Jin, Q. Wang, and S. Li, "Mechanism design of the minimally invasive vascular interventional surgery robot system," in *Proc. IEEE Int. Conf. Cybern. Intell. Syst. (CIS) IEEE Conf. Robot., Autom. Mechatronics (RAM)*, Ningbo, China, Nov. 2017, pp. 225–230.
[34] Z. Q. Feng, "Design and control of the master-slave minimally invasive vascular intervention robot system," Ph.D. dissertation, Dept. Control Theory Control Eng., Univ. Chin. Acad. Sci., Beijing, China, 2016.
[35] H. Y. Liu, "Study on the institutional design and master-to-master control of vascular intervention surgery robot," M.S. thesis, Dept. Mechatronic Eng., Yanshan Univ., Qinhuangdao, China, 2018.
[36] D. Huang, "Structure design and simulation analysis of vascular intervention surgery robot system," M.S. thesis, Dept. Mechatronic Eng., Yanshan Univ., Qinhuangdao, China, 2019.
[37] W. Zhang, "Study on the design and master control of vascular intervention surgery robot operation," M.S. thesis, Dept. Mech. Eng., Yanshan Univ., Qinhuangdao, China, 2015.
[38] H. Liu, "The establishment of catheter robot system and its key technology research," Ph.D. dissertation, Dept. Mech. Eng., Harbin Inst. Technol., Harbin, China, 2010.
[39] C. Ji, "The positioning and navigation of minimally invasive vascular intervention robot," Ph.D. dissertation, Dept. Control Theory Control Eng., Univ. Chin. Acad. Sci., Graduate School Chin. Acad. Sci., Beijing, China, 2011.
[40] X. Li, "Study on the surgical robot system of catheter guide wire intervention," M.S. thesis, Dept. Mech. Eng., Harbin Inst. Technol., Harbin, China, 2011.
[41] W. W. Yan, "Study on the design and control strategy of vascular intervention surgery robot," M.S. thesis, Dept. Control Sci. Eng., Huadong Jiaotong Univ., Nanchang, China, 2018.
[42] B. Chen, "Vascular intervention and motor control of remote operation robot based on force feedback," M.S. thesis, Dept. Instrum. Sci. Technol., Shanghai Jiaotong Univ., Shanghai, China, 2018.

HONGBO WANG (Member, IEEE) was born in Xingtai, Hebei, China, in 1956. He received the B.S. and M.S. degrees from the Institute of Northeast Heavy Machinery, Qiqihar, China, in 1982 and 1986, respectively, and the Ph.D. degree from Nagasaki University, Nagasaki, Japan, in 1997.

He has studied as a Visiting Scholar with the Institute of Robotics, ETH Zurich, Switzerland, from 1992 to 1993. After his Ph.D. degree, he has worked as a Researcher with Nagasaki University. In 1998, he has worked as the Deputy Manager of Daihen Corporation, Osaka, Japan. Since 2009, he has been working as a Professor with Yanshan University, Qinhuangdao, China. He has published approximately 150 papers in journals and international conferences. He has been granted more than 30 Chinese invention patents. Since 2010, he has presided over and undertook more than ten national projects. His major research interest includes robotics. His current research interests include surgical rehabilitation robots and assistance robots for the disabled and the elderly.

Dr. Wang is a member of the Chinese Association of Rehabilitation Medicine. He is also an Associate Editor of *International Journal of Intelligent Systems and Applications in Robotics*.

JINGYUAN CHANG was born in Hulunbuir, Inner Mongolia, in 1982. She received the B.S. degree in mechanical engineering and the M.S. degree in economics and management from Yanshan University, Hebei, China, in 2004 and 2012, respectively, where she is currently pursuing the Ph.D. degree in mechanical engineering.

In 2012, she worked at the Qinhuangdao Third Hospital. Her research interest includes the mechanism design and control methods of vascular interventional surgery robots.

HAOYANG YU was born in Heze, Shandong, China, in 1994. He received the B.S. degree in mechanical and electrical engineering from Hainan University, Hainan, China, in 2012. He is currently pursuing the M.S. and Ph.D. degrees in mechanical and electrical engineering with Yanshan University, Hebei, China.

His research interests include master-slave systems for remote surgical robots, force perception of surgical robots, and clinical applications of surgical robots.

HAIYANG LIU received the B.S. degree in vehicle engineering and the M.S. degree in mechanical and electrical engineering from Yanshan University, Qinghuangdao, Hebei, in 2015 and 2018, respectively.

He devotes himself to the design and research of robot structures.

CHAO HOU was born in Baoji, Shanxi, China, in 1987. He received the B.S. degree in mechanical engineering from Yanshan University, Hebei, China, in 2009, and the M.S. degree from the Xi'an University of Technology, Shanxi, in 2014. He is currently pursuing the Ph.D. degree in mechanical engineering with Tianjin University, Tianjin, China, and the Ph.D. degree with the Academy for Engineering and Technology, Fudan University.

He has worked as an Engineer with Jiangsu Hengrui Pharmaceutical Company Ltd., from 2014 to 2018. His research interests include intelligent medical robot, the mechanism design and control methods of vascular interventional surgery robots, and the mechanism design and control of rehabilitation robot.

HAIXIA LU was born in Datong, Shanxi, in 1995. She received the B.S. degree in mechanical engineering from Hohai University, Jiangsu, in 2018. She is currently pursuing the M.S. degree in mechanical engineering with Yanshan University.

Her research interest includes surgical robots.